Presented at the Society of Petroleum
Engineers California Regional Meeting,
Ventura, CA, April 18-20, 1979

LBL-8816 c.2

A PURELY NUMERICAL APPROACH FOR ANALYZING FLOW TO A WELL INTERCEPTING A VERTICAL FRACTURE

T. N. Narasimhan and W. A. Palen

March 1979

Prepared for the U. S. Department of Energy
under Contract W-7405-ENG-48

TWO-WEEK LOAN COPY

This is a Library Circulating Copy
which may be borrowed for two weeks.
For a personal retention copy, call
Tech. Info. Division, Ext. 6782

LAWRENCE BERKELEY LABORATORY
UNIVERSITY OF CALIFORNIA
BERKELEY

RECEIVED
LAWRENCE
BERKELEY LABORATORY

MAY 8 1979

LIBRARY AND
DOCUMENTS SECTION

LBL-8816 c.2

LEGAL NOTICE

This report was prepared as an account of work sponsored by the United States Government. Neither the United States nor the Department of Energy, nor any of their employees, nor any of their contractors, subcontractors, or their employees, makes any warranty, express or implied, or assumes any legal liability or responsibility for the accuracy, completeness or usefulness of any information, apparatus, product or process disclosed, or represents that its use would not infringe privately owned rights.

A PURELY NUMERICAL APPROACH FOR ANALYZING FLOW TO A WELL INTERCEPTING A VERTICAL FRACTURE

T. N. Narasimhan and W. A. Palen
Lawrence Berkeley Laboratory
Berkeley, California

ABSTRACT

A numerical method, based on an Integral Finite Difference approach, is presented to investigate wells intercepting fractures in general and vertical fractures in particular. Such features as finite conductivity, wellbore storage, damage, and fracture deformability and its influence as permeability are easily handled. The advantage of the numerical approach is that it is based on fewer assumptions than analytic solutions and hence has greater generality. Illustrative examples are given to validate the method against known solutions. New results are presented to demonstrate the applicability of the method to problems not apparently considered in the literature so far.

INTRODUCTION

The problem of fluid flow to a well intercepting a single vertical fracture is of considerable interest in the field of petroleum engineering. The transient pressure response of such a well to fluid production has been investigated by previous workers using analytical solutions, some of which are evaluated numerically. Despite their power, analytical methods have certain limitations. To overcome these limitations, numerical methods in conjunction with fast computing devices can be utilized with great advantage. The purpose of this paper is to describe and demonstrate the power of a fairly general numerical model in studying fluid flow to a well intercepting a vertical fracture.

The Problem

The problem of interest is schematically represented in Fig. 1. The reservoir is assumed to be homogeneous, horizontal, areally infinite and of thickness h. A vertical fracture of width w, length $2X_f$ and extending throughout the thickness of the reservoir and is fully penetrated by a well of radius r_w. It is assumed that the well produces fluid at a prescribed (usually constant) rate. The problem is to predict the pressure transient behavior of the system in general and the well in particular.

Previous Work

Although intere[illegible] wells intercepting vertical fractures dates [illegible]ck to 1960, the first comprehensive study of the pressure transient response of such a well was performed by Gringarten et al[1] who studied the case of flow to an infinitely conducting vertical fracture, with a hypothetical zero-radius well at its center. This and a few subsequent studies considered not only an infinite reservoir but also various types of bounded reservoirs. Later, Cinco-Ley et al[2] extended the Green's functions approach of Gringarten et al[1] to consider the more realistic cases of finite conductivity vertical fractures. In their studies, Cinco-Ley et al coupled the Green's function solution of the earlier work[1] with a one dimensional, linear solution for fluid flow within the fracture, the coupling procedure being subject to continuity of fluxes at the fracture surface. To evaluate their solutions, Cinco-Ley et al used a numerical method. In subsequent studies, Cinco-Ley and Samaniego[3] extended the solutions to include effects of wellbore storage and formation damage around the fracture.

Although they do discretize the fracture into several segments in their numerical evaluation, Cinco-Ley et al's method is basically analytic or at best semi-analytic in nature.

Limitations of Analytic Approach

The analytic approach has formed the backbone of well test interpretation and reservoir analysis since the 30's and has provided innumerable valuable insights in understanding reservoir response. Yet, tractable analytic solutions can be obtained only if the system under consideration is simple. Thus, the solutions so far presented in the literature consider : a) the reservoir is homogeneous b) the material properties are constant with time c) gravity effects are negligible and pressure gradients are small everywhere, and d) that the system is ini-

tially hydrostatic, meaning that pressure drawdown with reference to hydrostatic pressure, p_o, is zero everywhere in the system.

For handling realistic field problems, it is extremely desirable to have the ability overcome the aforesaid limitations. For example the assumption that material properties are independent of pressure, which is essential in order to be able to superimpose analytic solutions, may often be incorrect. In this connection it is quite well known that the permeability of a fracture is a strong function of its aperture and that fracture aperture is dependent on pore-fluid pressure.

A second assumption which reduces the generality of analytic solutions is that gravity is usually neglected. The investigations referred to in 1, 2, and 3 all define Darcy velocity in terms of pressure gradient, totally neglecting gravity. Although, from a physical point of view, such a definition of Darcy velocity is incorrect, petroleum engineers have traditionally used it with the assumption that the reservoir is thin and that, essentially, pressure is approximately equal to energy potential. This assumption has generally been reasonable since fluid pressure measurements were often subject to errors of about 7×10^{-2} MPa ($\approx$10 psi) or more. However, with the availability of sensitive pressure measuring devices and the existence of relatively thick reservoirs, the gravitational component may not be negligible and merits inclusion in the solution process (H. J. Ramey, personal communication.)

An alternate way to look at the equation of motion is that the pressure term used in Darcy's law by petroleum engineers actually denotes Δp rather than p. This is analogous to the practice in hydrogeology where the dependent variable in the diffusion equation is sometimes treated to be the drawdown rather than potential. This expression is valid provided that the system is initially assumed to be hydrostatic. Here again, the analytic solution approach is limited in applicability as it cannot easily handle arbitrary initial conditions.

Scope of Present Work

The aim of the present work is to demonstrate a numerical method in which the limitations of the analytic methods can be conveniently overcome. Intrinsically, the proposed computational model has very few assumptions built into it. We will first begin with a description of the proposed numerical model followed by a few typical examples serving to validate its applicability. We will conclude the paper with some new results which have not been published in the literature to our knowledge.

DESCRIPTION OF NUMERICAL MODEL

GOVERNING INTEGRAL EQUATION

The equation governing the flow of a slightly compressible fluid in a deformable porous medium is the well known equation of mass conservation. Consider a small domain ℓ of the flow region of interest. Let this subdomain, which has an abitrary shape, be small enough so that fluid potential and other properties do not vary rapidly over it so that one can define volume-averaged values of potential and other properties over it and associate these values with a nodal point interior to ℓ. Then, for this subdomain, one can write the mass conservation equation,

$$\rho G_\ell + \int_{\Gamma_\ell} \rho \frac{k}{\mu} (\rho g \nabla z + \nabla p) \cdot \vec{n} d\Gamma = M^*_{c,\ell} \frac{Dp_\ell}{Dt} \qquad (1)$$

in which G_ℓ is the volumetric rate of fluid generation from element ℓ, ρ is fluid density, k is intrinsic permeability, μ is dynamic coefficient of viscosity, g is gravity, z is elevation with reference to arbitrary datum, p is pressure, $\vec{n}$ is unit outernormal, $d\Gamma$ is a segment of the closed surface Γ_ℓ which bounds subdomains ℓ, $M^*_{c,\ell}$ is the fluid mass capacity of element ℓ defined as the mass of water required to change the average pressure over ℓ by unity (Narasimhan and Witherspoon[4]) and D/Dt is the material derivative. The element ℓ is so defined to always have a constant mass of solids, V_s so that the Darcy velocity in (1) denotes the mean velocity of water with reference to the solid grains.

In general, for a saturated-unsaturated porous medium, $M^*_{c,\ell}$ can be shown to be[4],

$$M^*_{c,\ell} = V_s \rho [e S c_w + S a_v + e \frac{dS}{dp}] \qquad (2)$$

in which c_w is volumetric compressibility of water S is fluid saturation, $a_v = (-de/d\sigma')$ where e is void ratio and σ' is effective stress. We make an implicit assumption here that $\Delta\sigma' = -\Delta p$. The first term within parenthesis in (2) denotes expansion of water, the second denotes skeletal deformation and the last, desaturation of pores.

In the problem that we are presently concerned with we are dealing with a fully saturated material for which S = 1 and dS/dp = 0. Hence (2) simplifies to

$$M^*_{c,\ell} = V_s \rho [e c_w + a_v] \qquad (3)$$

Note that $M^*_{c,\ell}$ denotes a generalized storage coefficient of the volume element ℓ. We could, for convenience, normalize $M^*_{c,\ell}$ with reference to the bulk volume of the element V_ℓ and divide through both sides of (3) by ρ and define the quantity, S^*_s which may be termed specific storage and defined as the volume of fluid released from a unit bulk volume of the element per unit change in pressure. Thus,

$$S^*_s = \frac{M^*_{c,\ell}}{V_\ell} = [\phi c_w + (1-\phi) a_v] \qquad (4)$$

If instead of a_v in (4) we wish to use c_f, the pore-volume compressibilility of the formation, then, noting that $c_f = (\frac{\phi}{1-\phi}) a_v$, we may rewrite (4) as

$$S^*_s = \phi [c_w + c_f] = \phi c_t \qquad (5)$$

which is the expression that is familiar to petroleum engineers.

In general, the coefficients in (1) are all functions of pressure or of time. Thus, G_ℓ can be an arbitrary function of time or pressure, ρ is a function of pressure through the equation of state, k is a function of pore geometry (hence, aperture) and $M^*_{c,\ell}$ is a function of pressure since e and a_v can both vary with stress.

Before we proceed further, it is instructive to relate (1) to the partial differential equation employed in references 1-3. To do this, we first divide both sides of (1) by V_ℓ and Δt and let $V_\ell \to o$. Then, in view of the basic definition of divergence[5] (1) reduces to,

$$g_\ell + \text{div}\,\frac{k}{\mu}\,(\rho g \nabla z + \nabla p) = S^*_s\,\frac{Dp}{Dt} \qquad (6)$$

where g_ℓ is the fluid generation rate (volumetric) per unit volume of the subdomain ℓ. If, in (6) we neglect gravity, and divide through by k/μ, we finally end up with the equation used in references 1-3,

$$\frac{\mu}{k}\,g_\ell + \text{div}\cdot\nabla p = \frac{S^*_s\mu}{k}\,\frac{Dp}{Dt} = \frac{\phi\mu c_t}{k}\,\frac{Dp}{Dt} \qquad (7)$$

DESCRIPTION OF NUMERICAL MODEL

The Integral Finite Difference Method

The Integral Finite Difference Method, hereinafter referred to as IFDM has been described elsewhere by Narasimhan and Witherspoon[6]. Basically, this method consists in discretizing the flow region into an appropriately large number of subdomains such that the potential varies linearly over each subdomain. The volume-averaged potential over each subdomain is associated with a representative nodal point interior to each subdomain. The discretization is so carried out that the line joining nodal points of neighboring elements is normal to the interface in between. To each subdomain, the conservation equation is directly applied, subject to compatibility of fluxes and potentials between adjoining elements. The gradient in potential between adjoining elements is evaluated using the simple concept of finite differences.

The discretized equivalent of (1) may now be written as[7],

$$\rho G_\ell + \sum_m \rho\frac{k}{\mu}\,\frac{\rho g(z_m - z_\ell) + (p_m - p_\ell)}{D_{\ell,m}}\,\Gamma_\ell = M^*_{c,\ell}\,\frac{\Delta p_\ell}{\Delta t} \qquad (8)$$

where m denotes all the subdomains communicating with ℓ, $D_{\ell,m}$ is the distance between nodal points ℓ, m and $\Gamma_{\ell,m}$ is the area of the interface between ℓ and m. Note that if $\Gamma_{\ell,m}$ coincides with the external boundary of the flow region for some m, then for that m either p_m or the entire flux term is known from boundary conditions.

Temporal Discretization

In (8) both p_m and p_ℓ vary with Δt and for maximum accuracy one should use their mean values defined by

$$\bar{p}_m = p^o_m + \lambda\Delta p_m \qquad (9a)$$

$$\bar{p}_\ell = p^o_\ell + \lambda\Delta p_\ell \qquad (9b)$$

where the bars denote mean values over Δt, the superscript o denotes the known initial value and $0 < \lambda < 1$ denotes a weighting function. $\lambda = 0$ results in an explicit equation while $\lambda = 0.5$ and $\lambda = 1$ respectively correspond to Crank-Nicholson and backward differencing approximations. The set of difference equations resulting from (8) and (9) are written in a mixed explicit implicit form which is then solved by a point iterative scheme using an accelaration factor. For details the reader is referred to Narasimhan et al[7].

Non-Linear Coefficients

In equation 1 the parameters G_ℓ, k, and $M^*_{c,\ell}$ are all functions of pressure and time, in general. So also are the boundary conditions. In the computational algorithm, all these non-linear coefficients are handled in a quasi-normalized form. That is, using the past history of pressure variation over the system, a reasonable mean value of pressure is estimated for each subdomain and the coefficients are evaluated at these estimated values of pressure. For purely time dependent variations such as the source term or boundary conditions, the parameters are estimated for an instant midway through Δt. Since, in a saturated domain both k and $M^*_{c,\ell}$ are strongly governed by skeletal structure, and since skeletal structure is dependent on effective stress rather than pore fluid pressure, the pore pressures are first converted to σ' using the effective stress law, $\sigma' = \sigma - p$ before evaluating k and $M^*_{c,\ell}$. The effective stress law used here uses the simple one-dimensional consolidation theory of Terzaghi (1925)[8].

Some Advantages of the Numerical Method

In as much as the proposed numerical method solves the governing equation in the most primitive form, it has very few assumptions built into it. Thus there is greater freedom to handle realistic field problems involving complex geometry and arbitrary heterogeneity. Secondly, because (1) is basically a non-linear equation, the numerical method can provide solutions to problems such as those involving deformable fractures. The method of superposition of analytic solutions is not valid for such non-linear problems. Also, as compared with the analytic solutions, the numerical model gives due consideration to gravity. Finally, the IFDM can easily handle three-dimensional problems if required.

Among the disadvantages of the numerical method one could mention the following. Each given situation may have to be treated as a specific problem increasing the effort involved in the solution process. Also, each problem requires the preparation of a mesh of elements, the number of mesh points varying from problem to problem due to property variations and depending upon the accuracy desired. Input data preparation may often consume significant time and effort. In rare instances, the validity of the numerical solution may not be amenable to easy check.

Details of Simulation

The investigation consisted of two sets of simulations, the first set consisting of validation problems and the second consisting of new problems

apparently unreported in the literature. The details of phenomena investigated in each set are given below.

Validation problems: Finite conductivity vertical fracture; effects of wellbore storage and damage.

New problems: Unequal wing-length; choked fracture; deformable fracture; effect of fracture storativity.

Mesh Used

For purposes of this study, the horizontally infinite reservoir was treated as a two-dimensional flow region with unit thickness in the third direction. On grounds of symmetry, only one-quarter of the flow region needed simulation in all cases except the unequal wing-length problem in which one-half of the flow region was simulated. The IFDM mesh used is shown in Figure 2, in which the mesh detail increases as one proceeds from the top to the bottom. The volume elements have been so designed as to roughly conform to the expected pattern of fluid flow. Thus, the elements are arcuate close to the well and around the fracture edge to efficiently simulate the radial flow. As one proceeds away from the well, the arcuate elements gradually lose their curvature to become rectangular elements close to the fracture and elsewhere to simulate the expected, relatively rectilinear flows. In the mesh the fracture itself is treated as one or more volume elements with finite volume, surface area and fluid mass capacity. In terms of magnitude, all the simulations were carried out with x_f = 10m (32.58 ft). For all cases except the deformable fracture case, the fracture aperture w was fixed at 0.01m (0.39 in). For the deformable fracture case the aperture was initially set at 0.001m (0.039 in). Fluid was allowed to enter the well through the fracture as well as through the well casing (if needed). Fluid was allowed to enter the fracture through its edges.

As can be seen from the figure, the volume elements are widely variable in size varying from about 2 x 10^{-2} m^3 for the smallest fracture element to more than 2 x 10^3 m^3 for the largest element at the periphery. The total number of elements varied around 225 depending on the particular case studied. Depending on the contrast in permeability between the formation and the fracture, the fracture was discretized into volume elements varying in number from 2 to 12.

For cases in which wellbore storage had to be neglected to simulate analytic solutions, the well radius was assumed be r_w = 0.005m (.02in). In other cases wellbore radius was fixed as needed. All the simulations assumed wellbore storage due to fluid level changes in the well.

Parameters Used

The parameters critical to the present study are: formation permeability k; formation storativity, S_s^* $(=\phi c_t)$; fracture permeability, k_f, and fracture storativity, $S_{s,f}^*$ $(=\phi c_t)_f$. In addition, for particular cases, the permeability of the skin, k_s or the permeability of the choke, k_{ch} are also important.

In all the simulations, the reservoir was assumed to be of practically infinite areal extent The program, however, is general enough to handle any type of time dependent boundary condition. All the simulations were carried out with fixed flow rate from the well.

The parameters used in the simulation are given in Table I.

In the interpretation and comparison of the results of the simulations, the following dimensionless variables are important:

Dimensionless time, $t_{Df} = \dfrac{kt}{\phi\mu c_t X_f^2}$ (10)

Dimensionless well-drawdown $P_{wD} = \dfrac{2\pi kh\Delta p}{q\mu}$ (11)

Dimensionless fracture conductivity $C_r = \dfrac{wk_f}{\mu k X_f}$ (12)

Dimensionless wellbore storage $\bar{C} = \dfrac{c}{2\pi\phi c_t X_f^2}$ (13)

Dimensionless fracture skin $S_{fs} = \dfrac{\pi}{2}\dfrac{w_s}{X_f}\left(\dfrac{k}{k_s} - 1\right)$ (14)

VALIDATION OF NUMERICAL METHOD

Finite Conductivity Fracture

The first set of validation runs consisted in studying the effect of varying the conductivity of the fracture on the pressure transient response of the system. The solutions generated were compared with the semi-analytical solutions of Cinco-Ley et al[2]. The results of these simulation are presented in Figure 3 in the form of a log-log plot of t_{Df} versus P_{wD} for different values of C_r. Note from the definition of C_r that if the other parameters are held constant, C_r is directly related to k_f.

In figure 3 solutions are presented for four values of C_r: 0.2, 1, 10. 100. The Case, C^r = 100 practically coincides with the infinite conductivity case while C_r = 0.2 corresponds to a k_f which is 500 times smaller than that of C_r = 100. Comparison of the analytic and numerical solutions presented reveal three interesting features. First, there is excellent agreement between the numerical solutions and those of Cinco-Ley et al[2] over most of the range of t_{Df}. The second is that for t_{Df} > 30, all the four numerical results depart noticeably from the Cinco-Ley et al solution due to the fact that outer boundary of the mesh used corresponds as a barrier boundary. Finally, in the particular case of C_r = 0.2, the numerical results differ from the semianalytic solution for t_{Df} < 0.01. This departure, which is noticeable because of the low k_f, is due to the effect of the finite value of r_w = 0.005m which was used in the numerical simulation.

For values of t_{Df} exceeding 10, the system behaves essentially like a radial flow system with an equivalent well with a radius equal to 1/4 x_f(Prats et al.[9]). For values of t_{Df} < 10^{-4}, the system is dominated by well-bore storage (unit slope). At this level, C_r cannot be accurately

used as a unique parameter because of the fact that at small times only a portion of the fracture close to the well-bore will see the effects of fluid production. The parameter, C_r which has x_f included in its definition cannot be meaningfully defined until such time when the pressure transient has migrated to the edge of the fracture so that the entire fracture participates in transient fluid flow. Thus, in our future discussions we need to restrict ourselves only over the range 10^{-4} to 10 for t_{Df}.

Effect of Well-bore Storage

The influence of wellbore storage on pressure drawdown is very clearly seen in Figure 4. In this figure, P_{wD} is plotted as a function of t_{Df} for different values of the wellbore storage parameter, $\bar{C}$ which is defined in (13). In (13), $\bar{C}$ is the volume of fluid released from the wellbore per unit change in wellbore fluid pressure. All the curves in Figure 4 pertain to a $C_r = 100$.

The zero-wellbore-storage solution of Cinco-Ley et al[2] is represented by the upper most line in Figure 4. This curve is very closely matched by the numerical result for $\bar{C} = 1.25 \times 10^{-3}$ which corresponds to a r_w of 0.005m. As can be seen from the figure, wellbore storage effects persist up to a value of $t_{Df} = 10$ for $C_r = 0.5$. In the problem studied, $C_r = 0.5$ corresponds to a $r_w = 0.10$m (4 in) and $t_{Df} = 10$ corresponds to 10^5 secs (1.16 days). It is obvious that in realistic field situations one may have to use packers to reduce wellbore storage effects. Also, it can be demonstrated that the effects of wellbore storage will persist for a longer period as fracture permeability decreases.

Fracture-Skin

It is quite well-known that formation damage around a wellbore can be quantitatively handled with a skin factor. So also one can define a similar skin concept for damage around a fracture. Thus Cinco-Ley and Samaniego[3] define a fracture skin, S_{fs} by the relation given in (14) in which w_s is the width of the skin and k_s is the permeability of the skin. The effect of S_{fs} on P_{wD} for $C_r = 100$ is demonstrated by the family of curves shown in Figure 5. The upper four curves and the Cinco-solution in this figure pertains to a $r_w = 0.005$m (0.2 in) while the two lower curves pertains to a $r_w = 0.076$m (3 in). The mathematical representation of the finite-width skin is shown as an inset in Figure 5.

Three points of interest may be noticed in Figure 5. First, the effect of wellbore storage becomes more pronounced as S_{fs} increases, since higher S_{fs} implies a general degradation of permeability around the well. Second, there is a slight discrepency between the Cinco-Ley[3] solution and the solution of this study for $S_{fs} = 0.1$, for $t_{Df} < 10^{-2}$. This is consistent with Cinco-Ley and Samaniego[3] who considered an infinitesimal skin. However, they do state in their paper that a skin of finite width should be expected to produce a slightly different well-response at early times. In other words, for the same S_{fs}, different combinations of k_s and w_s should lead to different P_{wD} versus t_{Df} relation for small values of time. To verify this, a second simulation was carried out in which the width of the skin was increased by a factor of two over the value used for the results presented in Figure 5. A comparison of the two different finite-width skin solutions are given in Figure 6. It can be seen from Figure 6, that as the width is increased for a constant S_{fs}, the curves tend to move down on the log-log paper. The final feature worthy of note in Figure 5 is that as the well-bore radius is increased, to represent realistic field cases, the early-time details (up to $t_{Df} = 10$) are so completely masked that the utility of the S_{fs} parameter in interpretation is curtailed.

Some Points of General Interest

Before we pass on to the the consideration of new results, it is of interest to discuss a few special aspects relating to the results presented so far.

The first of these is the optimum number of elements into which the fracture is discretized for purposes of simulation. As is obvious, the number of elements should be increased as the fracture conductivity decreases and the gradient of potential within the fracture becomes significant. Conversely, as the conductivity of the fracture becomes infinite, the entire fracture can be treated as a single element or even as an intrinsic part of the well. In the simulations, we used two fracture elements for $C_r = 100$ and 10; 10 fracture elements for $C_r = 1$ and 12 fracture elements for $C_r = 0.2$. The drawback in using a large number of elements for higher values of C_r is that the higher conductivity greatly decreases the stable time step for the fracture elements resulting in greatly enhanced computational effort. On the other hand, reducing the number of elements for lower values of C_r leads to loss of accuracy. The optimum number of elements depends on the fracture surface area, fracture storativity and the contrast between k and k_f. Although, in the present study, the number of fractures were chosen based on trial and error, it should not be difficult to formulate a rational criterion for deciding on the same.

A second point of interest concerns the manner in which the flow at the edge of the fracture is handled. In all the simulations the edge was assumed to be rectilinear with fluid entering the fracture through the narrow end. Examination of the computer outputs showed that about one percent of the total flux entering the fracture entered through the end. Although the total flux is small, the velocity of entry at the fracture was always found to be very high due to the narrowness of the opening. Considering the fact that little is generally known about the geometry of the fracture edge we need not concern ourselves any more with that topic apart from stating that the actual flux through the end depends very much on its geometry.

Finally, a brief mention about flow across the wellbore. Careful examination of the results indicated that the quantity of fluid entering the wellbore increases with increasing wellbore radius and decreasing fracture conductivity. In general, the quantity of water entering the well through the region outside of the fracture is not more than about one-percent when a realistic wellbore radius is assumed.

NEW RESULTS

We now pass on to consider some new results that were generated during the present study.

Effect of Fracture Storativity

The solutions so far discussed are based on the assumption that fracture storativity $(\phi c_t)_f$ is the same as formation storativity, ϕc_t. The effect of varying $(\phi c_t)_f$ from 10^{-9} m^2/Newton to 10^{-7} m^2/Newton on P_{wD} is shown in Figure 7. In all the three cases an r_w = 0.005m was assumed. As can be seen from the figure, for the particular conditions used in the study, changing (ϕc_t) from 10^{-9} to 1^{-8} m^2/Newton did not significantly change the fluid mass capacity of the fracture so that these two solutions are almost identical. However, when $(\phi c_t)_f$ is increased to 10^{-7} m^2/Newton, the fracture capacity becomes comparable in magnitude to wellbore storage, there by causing a significant change in the pressure transient behavior.

Unequal Wing-length

It is customarily assumed that hydraulic fracturing at depth creates an opening symmetrical about the wellbore. However, it is conceivable that fracture is initiated in only one direction (single-wing; see inset Figure 8) or that it propagates only partially due to rock inhomogeneities. Recent field studies[10] support this suspicion. That the unequal wing-length problem may be of interest was suggested some years ago by Raghavan of the University of Tulsa. Our investigation of the problem is summarized in Figures 8, A, B and C. In as much as an asymmetrical wing requires the simulation of one-half of the flow region, and since a symmetrical wing requires only one-quarter of the flow region, two different meshes were designed to appropriately handle the single-wing and one and one-half wing cases.

Figures 8 A, B and C show drawdown behaviors for C_r = 1, 10 and 100 with one wing, one and one-half wing and two wings. In all cases, the undamaged well had an r_w = 0.005m, corresponding to a $\bar{C} = 1.25 \times 10^{-3}$.

In all cases, the drawdown for the single-wing condition is quite distinct from those of the one and one-half- and two-wing conditions. This is due to the decrease in overall permeability on the unfractured side. While the difference between the one and one-half- and two-wing case is distinct at C_r = 100, it is not so clear low t_{Df} at C_r = 10 and disappears below $t_{Df} = 10^{-2}$ for the tight fracture case (C_r =1). This is to be expected since, in tight fracture cases, flow is governed by the well-bore end of the fracture. Indeed, other results generated during the present study showed that for C_r = 0.2, reducing the permeability of the further half of the fracture by an order of magnitude had little effect on the pressure-transient response of the well-bore.

The similarity in the shapes of the curves in Figure 8 raises the basic question of reliably determining fracture geometry and fracture permeability by type-curve matching procedures. The solution is obviously non-unique and the type curves have to be used with caution and judgement in the light of geological knowledge of the near-well regime.

Choked Fracture

If the proppant is not uniformly distributed in the fracture, it is conceivable that permeability variations may occur along the crack, most likely near the well bore. The importance of a fracture which is choked close to the well-bore was pointed out to us recently by Alain Cringarten of Flopetrol in France. Our brief study of this problem is summarized in Figure 9. In all the four cases given in the figure, the X_{ch}, the choke length was assumed to be 8 percent of X_f. As can be seen from the figure the pressure transient behavior at the well changes dramatically in the case of r_w = 0.005m, as the choke permeability decreases, confirming that prevention of choking is essential to well-economics. However, it is also noticed from the bottom curve in the figure that a realistic well of 0.0762m diameter (6" diameter) can completely mask the early-time effects of choking. Note also that when k_{ch} is low (.001 k_f) wellbore storage effects are discernible up to t_{Df} = 0.001.

Deforming Fracture

Thus far we have considered rigid fractures with constant k_f and $(\phi c_t)_f$. Realistically, however, it is possible that proppant crushing may occur, resulting in fracture deformation with pore-pressure change. For convenience, we may term such a fracture to be "breathing". The k_f and $(\phi c_t)_f$ of a breathing fracture are functions of the effective fracture stresses. thus one can define the fracture aperture as a function of σ' in the manner proposed by Narasimhan and Witherspoon[4],

$$w = w_o - (\sigma' - \sigma'_o)\, a_v \qquad (15)$$

Also, in the manner suggested by Iwai[11], k_f can be treated as a quadratic function of w by the relation

$$k_f = \frac{w^2}{12} \qquad (16)$$

The incorporation of fracture deformation into the governing equation renders it non-linear and invalidates the superposition procedures normally employed in analytic solutions. The method proposed in the present study was used to investigate, in a preliminary fashion, the pressure transient behavior of a well intercepting a breathing fracture. The results generated using the following parameters are given in Figure 10:

k_f = $w^2/12$

a_v = 1.3×10^{-10} m^2/N

$w_{initial}$ = 10^{-3} m

Z = 2,000 m

Po = 1.959×10^7 N/m^2

The above parameters have been chosen more with a view to demonstrating the applicability of the method than to simulate a very realistic field case. In Figure 10, the breathing fracture solution is shown compared with two supposedly limiting rigid fracture solutions. Thus, the solution for $C_r = 26.2$ roughly corresponds to a rigid fracture with the initial assumed fracture aperture while the case, $C_r = 1.0$ roughly corresponds to the average fracture aperture at $t_{Df} = 10$ for the breathing fracture case. As can be seen from the figure, the breathing fracture solution starts off with the solution for $C_r = 26.2$ at $t_{Df} = 10^{-2}$ and, with time, approaches the other limiting solution for $C_r = 1$. For $t_{Df} < 10^{-2}$ the breathing fracture solution lies slightly below the solution for $C_r = 26.2$. This seemingly anomalous behavior can be explained by the fact that a rigid fracture capacity is governed purely by the expansion of water while a breathing fracture has far higher storage due to the added fracture deformation coefficient.

CONCLUSIONS

The Integral Numerical Method described in this paper provides an efficient, general purpose tool for studying the presure transient response in finite diameter wellbores intercepting rigid or deforming fractures. The results presented not only validate the method in the light of already published literature, but also reveal new results and their implications in respect of problems not hitherto presented to our knowledge.

NOMENCLATURE

a_v coefficient of compressibility

c wellbore storage constant = volume of fluid released from wellbore due to unit change in pressure

c_f pore volume compressibility of the formation

c_t "total" system compressibility

c_w water compressibility

C_r dimensionless fracture conductivity $= \frac{wk_f}{\pi k X_f}$

$\bar{C}$ dimensionless wellbore storage constant $= c/2\pi\phi c_t X_f^2$

e void ratio

e_o void ratio at reference effective stress σ'_o

g gravitational constant

g_ℓ volumetric fluid generation rate per unit volume of ℓ

G_ℓ volumetric fluid generation rate

h height of fracture and formation

k permeability

k_{ch} choked fracture permeability

k_f fracture permeability

k_s formation skin damage permeability

$M^*_{c,l}$ fluid mass capacity of a finite subregion; conceptually a generalized storage coefficient

p_ℓ, p_m average pressure in element ℓ, m

p^o, p^o_m initial pressure in element ℓ, m

p pressure

p_f fracture pore pressure

p_o reference pressure

p_{wD} dimensionless wellbore pressure drop

Δp drawdown; difference between p_{static} and $p_{flowing}$

q well pumping rate

r_w wellbore radius

S saturation

S_{fs} fracture skin damage coefficient $= [\frac{\pi}{2}\frac{w_s}{X_f}](\frac{k}{k_{fs}-1})$

S^*_s specific storage (ϕc_t)

$t, \Delta t$ time, change in time from initial time

T_{Df} dimensionless time $= k\rho g\Delta t/\mu S^*_s X_f^2$

V volume

V_ℓ bulk volume of element ℓ

V_s solids volume

V_v void volume

w fracture width

w_o fracture width at reference stress

w_s fracture formation damage thickness

X_f fracture wing length

z elevation

Z formation depth below land surface

γ specific weight of water

Γ_ℓ bounding surface of element ℓ

λ weighting factor

μ fluid viscosity

ρ density

σ total stress

σ' effective stress $= -p_f$

ϕ porosity

λ weighting factor

μ fluid viscosity

ρ density

σ total stress

σ' effective stress $= -p_f$

ϕ porosity

ACKNOWLEDGMENTS

We would like to thank Ravi Narasimhan for help with computer graphics. This work was supported by the Division of Geothermal Energy of the U.S. Department of Energy under Contract No. W-7405-Eng-48.

REFERENCES

1. Gringarten, A.C., Ramey, H.J., Jr., and Raghavan, R. Unsteady-state pressure distributions created by a well with a single infinite-conductivity vertical fracture. Soc. Pet. Eng. J., August 1974, 347-360.

2. Cinco-Ley, H., Samaniego, V.F., and Dominquez, A.N. Transient pressure behavior for a well with a finite-conductivity vertical fracture. Soc. Pet. Eng. J., August 1978, 253-264.

3. Cinco-Ley, H., and Samaniego, V.F. Effect of wellbore storage and damage on the transient pressure behavior of vertically fractured wells. SPE 6752 presented at the 52nd annual fall Technical Conference and Exhibition of the Society of Petroleum Engineers, Denver, Colorado, 9-12 October 1977.

4. Narasimhan, T.N., and Witherspoon, P.A. Numerical model for saturated-unsaturated flow in deformable porous media. 1: Theory. Water Resources Res., June 1977, 13(3), 657-664.

5. Sokolnikoff, I.S., and Redheffer, R.M. Mathematics of physics and modern engineering. New York: McGraw-Hill, 1966.

6. Narasimhan, T.N., and Witherspoon, P.A. An integrated finite difference method for analyzing fluid flow in porous media. Water Resources Res., February 1976, 12(1), 57-64.

7. Narasimhan, T.N., and Witherspoon, P.A. Numerical model for saturated-unsaturated flow in deformable porous media. 2: The algorithm. Water Resources Res., April 1978, 14(2), 255-261.

8. Terzaghi, K. Principle of soil mechanics: A summary of experimental results of clay and sand. Eng. News. Res., 1925, 3-98.

9. Prats, M., Hazebroek, P., and Strickler, W.R. Effect of vertical fracture on reservoir behavior --compressible fluid case. Soc. Pet. Eng. J., June 1962, 87-94.

10. Smith, M.B., Holman, G.B., Fast, C.R., and Covlin, R.J. The asimuth of deep, penetrating fractures in the wattenberg Field. Jour. Pet. Tech., 1978, 185-193.

11. Iwai, K. Fundamental studies of fluid flow through a single fracture. PhD Dissertation, Department of Civil Engineering, University of California, Berkeley, 1976.

Table 1

Parameters Used in Simulation

Parameter	SI units	Conventional units
k	$1.0197\ (10^{-13})\ m^2$	.103 Darcy
S_s, S_{sf}	$10^{-4}\ p_a^{-1}$	$6.897 \cdot 10^{-1}\ psi^{-1}$
X_f	10 m	32.8 ft
w	.01 m	.33 ft
V_w	.005 m	1.27 in
z	100 m	328 ft
h	1 m	3.28 ft
w_s	.2 m	$6.56\ 10^{-1}$ ft
k_f	$3.204\ (10^{-8})\ m^2$	$3.25 \cdot 10^4$ Darcy
q	$6.2832\ (10^{-3})\ m^3/sec$	341 bbls/day
g	$9.807\ m/sec^2$	32.2 ft/sec
μ	10^{-3} kg/m-sec	.1 cp
ρ	$10^3\ kg/m^3$	$62.416/ft^3$
ρ_s (overburden)	$2.10^3\ kg/m^3$	$125\ lb/ft^3$
p_z	$1.96\ 10^6$ Pa	285 psi

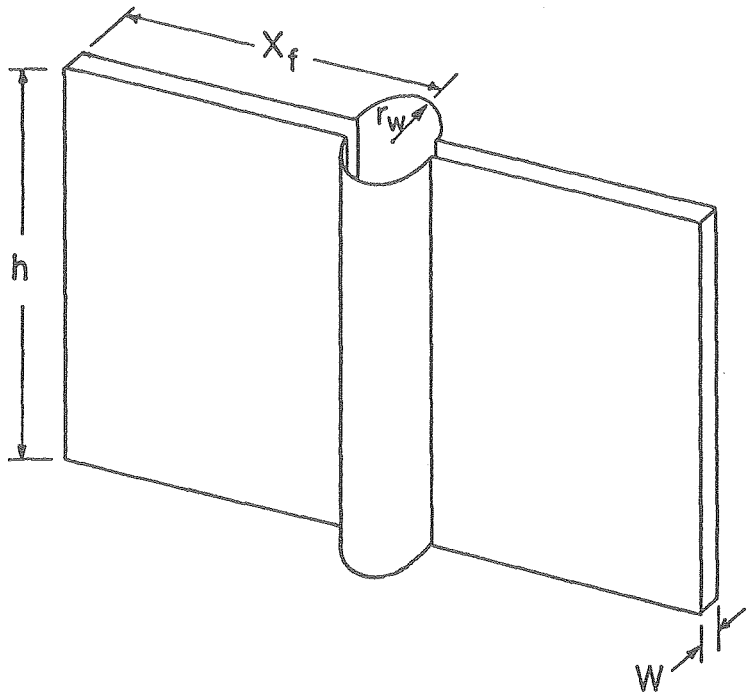

XBL 792-5743

Fig. 1. Representation of a Vertical Fracture Intercepting a well.

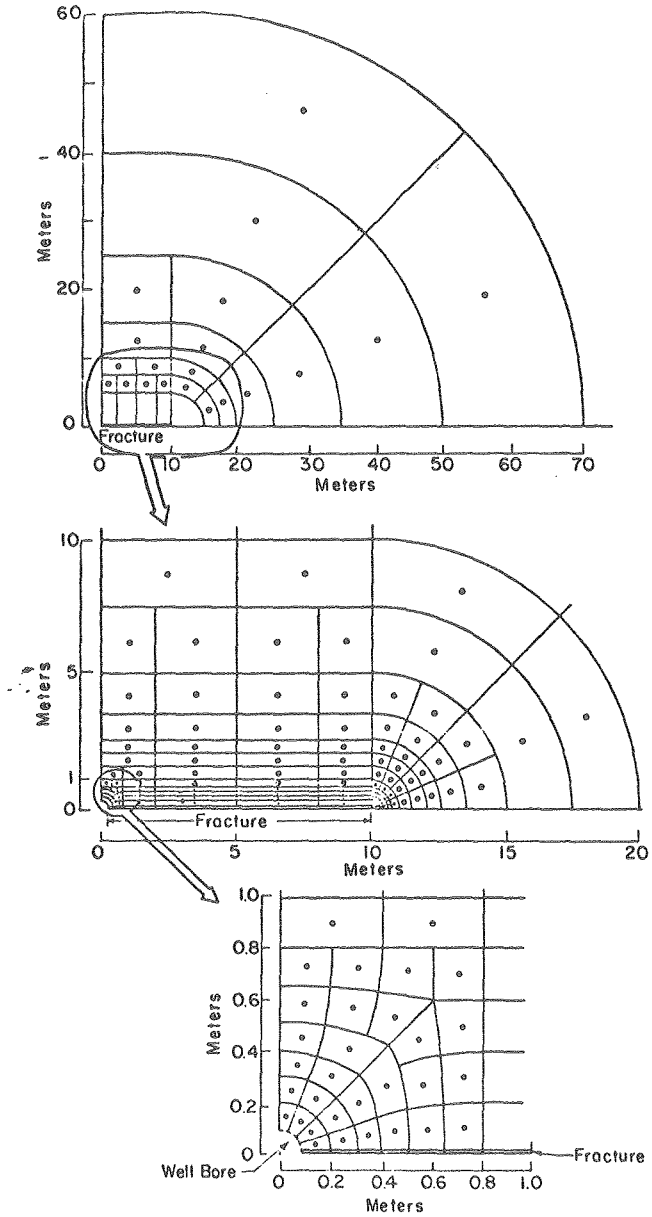

XBL 792-5744

Fig. 2. IFDM Mesh Used for Simulating Flow to a Well Intercepting a Vertical Fracture.

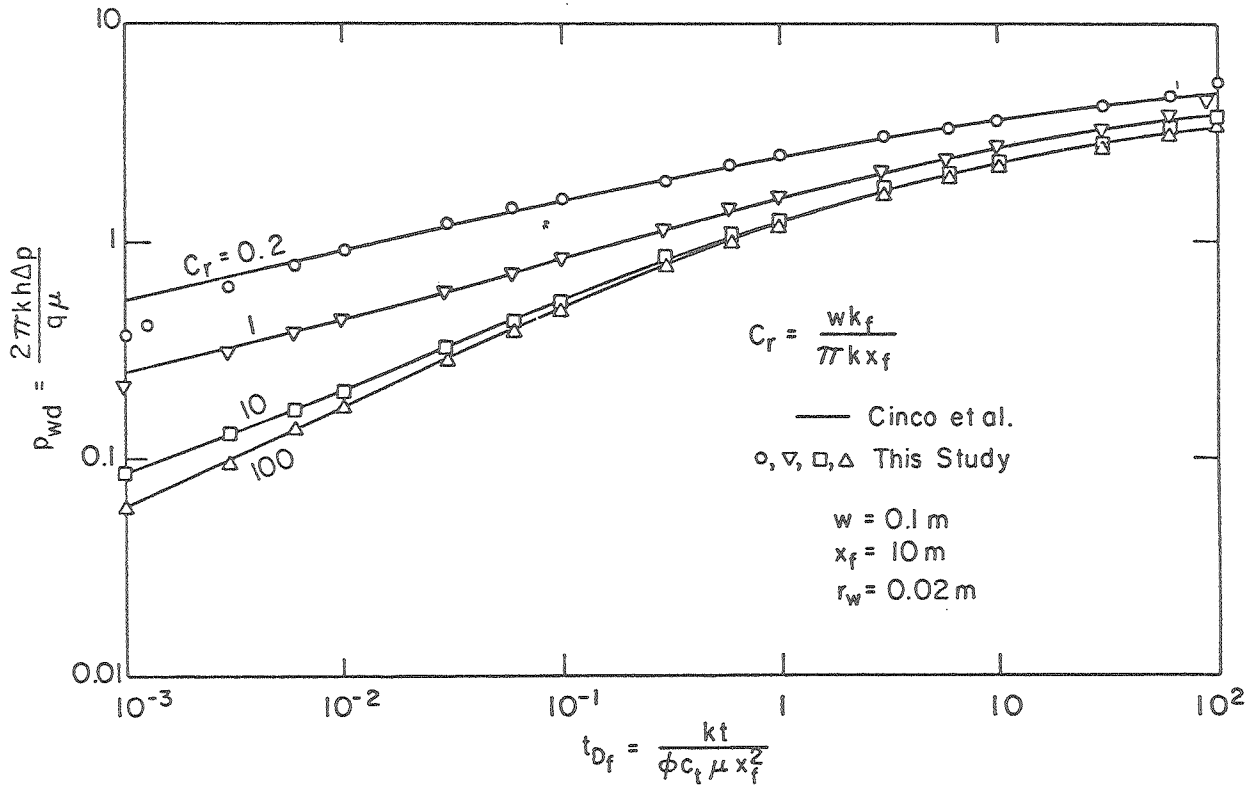

XBL 792-5741

Fig. 3. Log-Log Plot of P_{wD} vs T_{Df} for Various Values of Cr: Comparison of Numerical and Analytical Results.

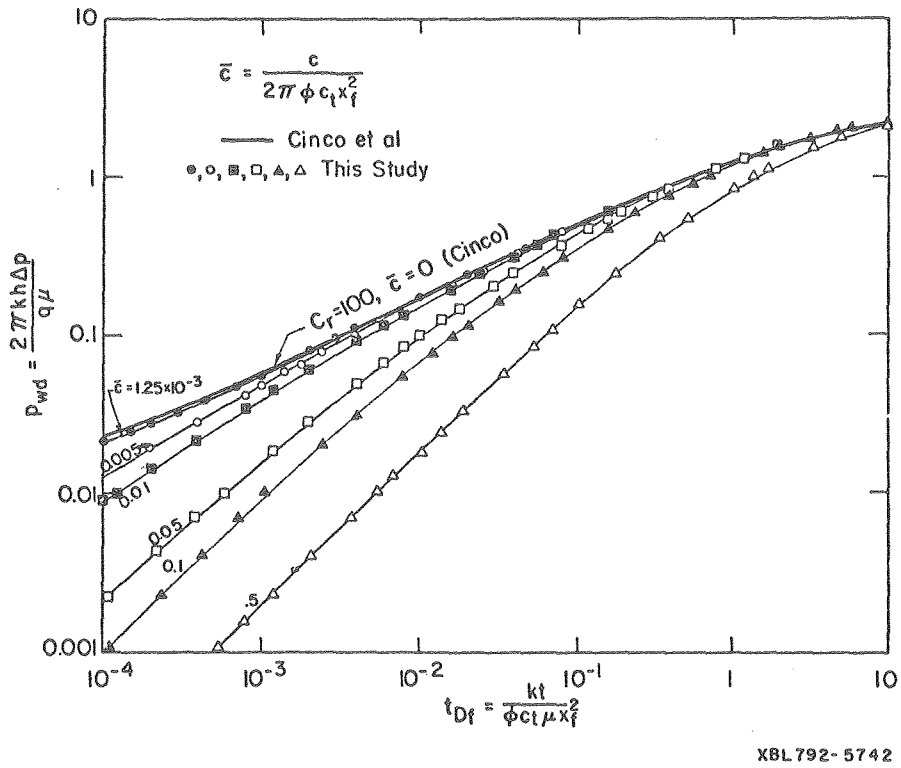

Fig. 4. Log-Log Plot of P_{wD} vs T_{Df} for Various Values of $\bar{C}$; for a Constant Value of Cr = 100.

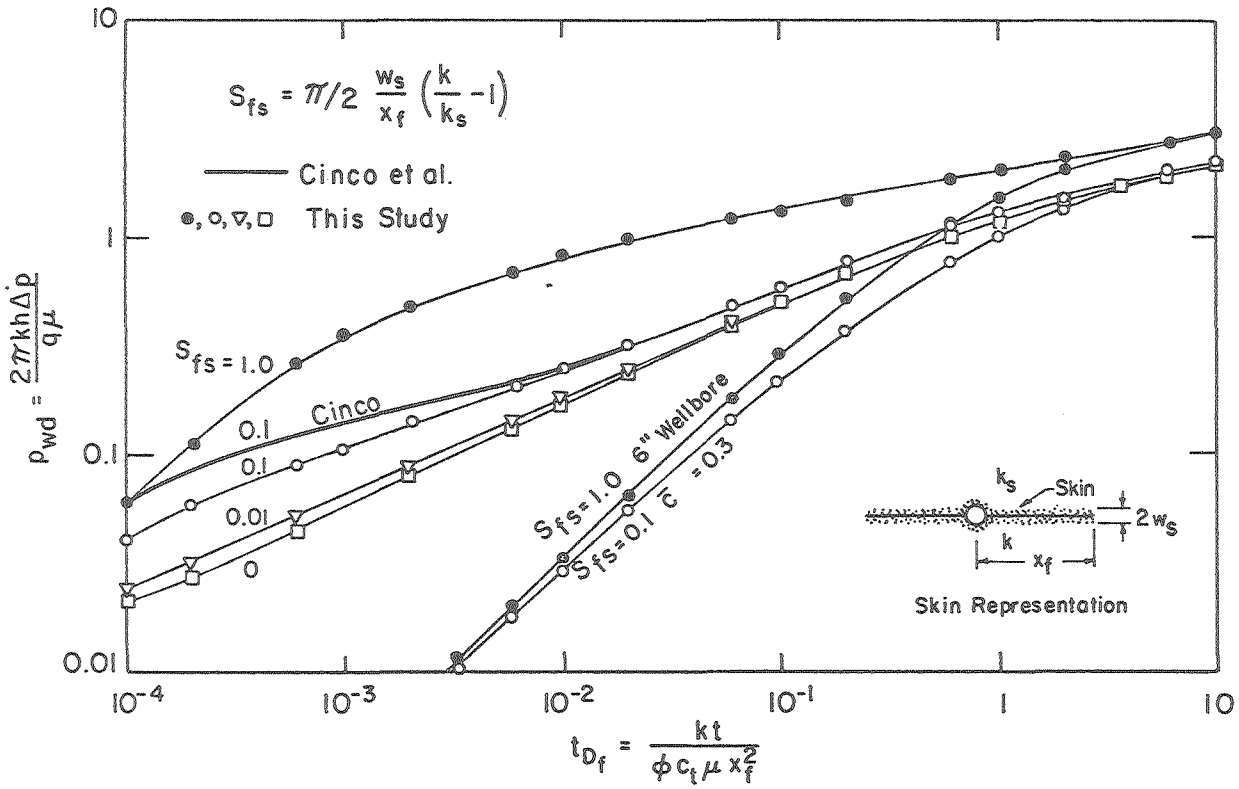

Fig. 5. Log-Log Plot of P_{wD} vs T_{Df} for Various Values of S_{fs}; for a Constant C_r = 100 and Wellbore Radii of .005m (.2 inch) and .076m (3 inches). XBL792-5740A

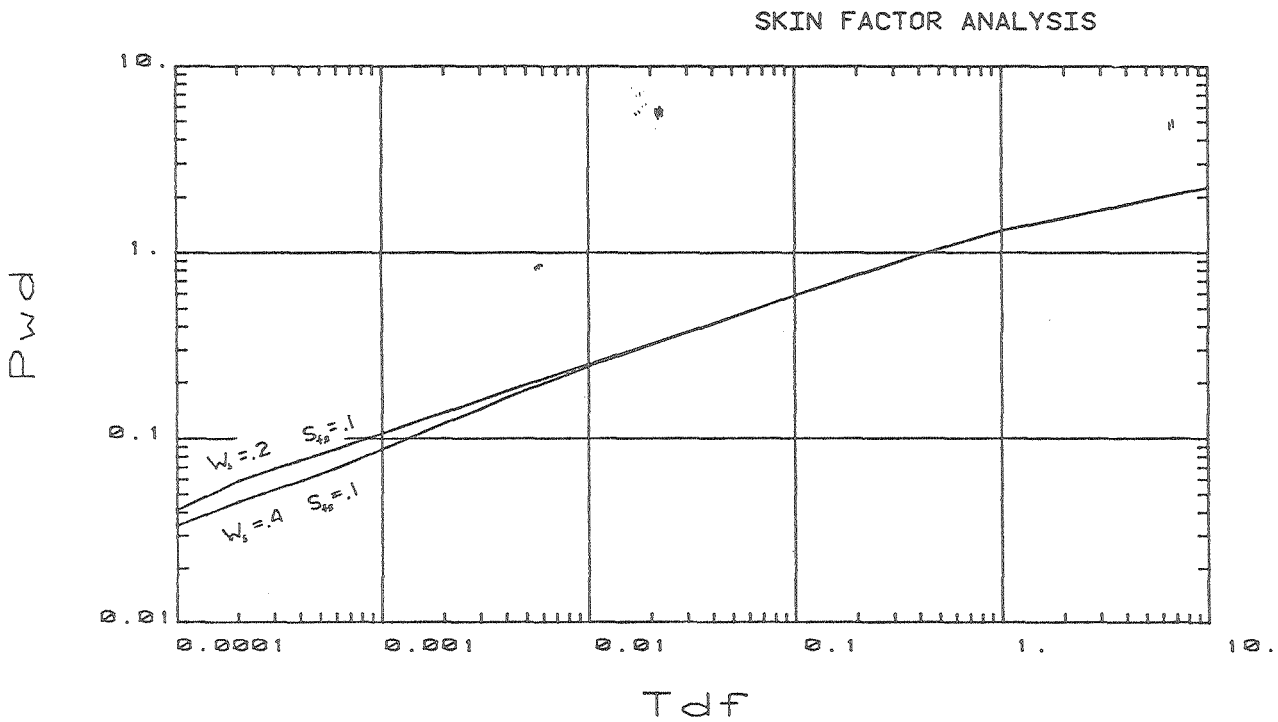

XBL 792-8501

Fig. 6. Log-Log Plot of P_{wD} vs T_{Df} for Constant S_{fs} = .1 and Different Values of Finite Width W_s and K_s.

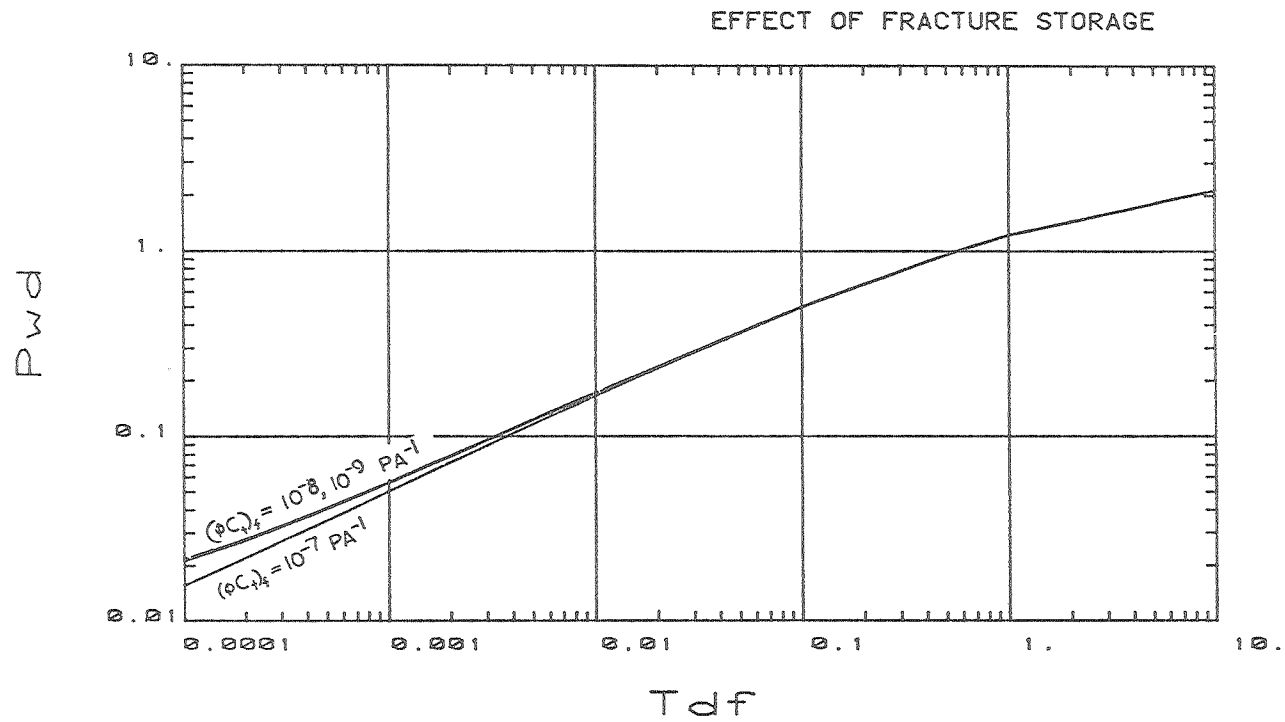

XBL 792-8502

Fig. 7. Log-Log Plot of P_{wD} vs T_{Df} for Constant C_r = 100 and Variable $(\phi c_t)_f$; r_w = 0.005m.

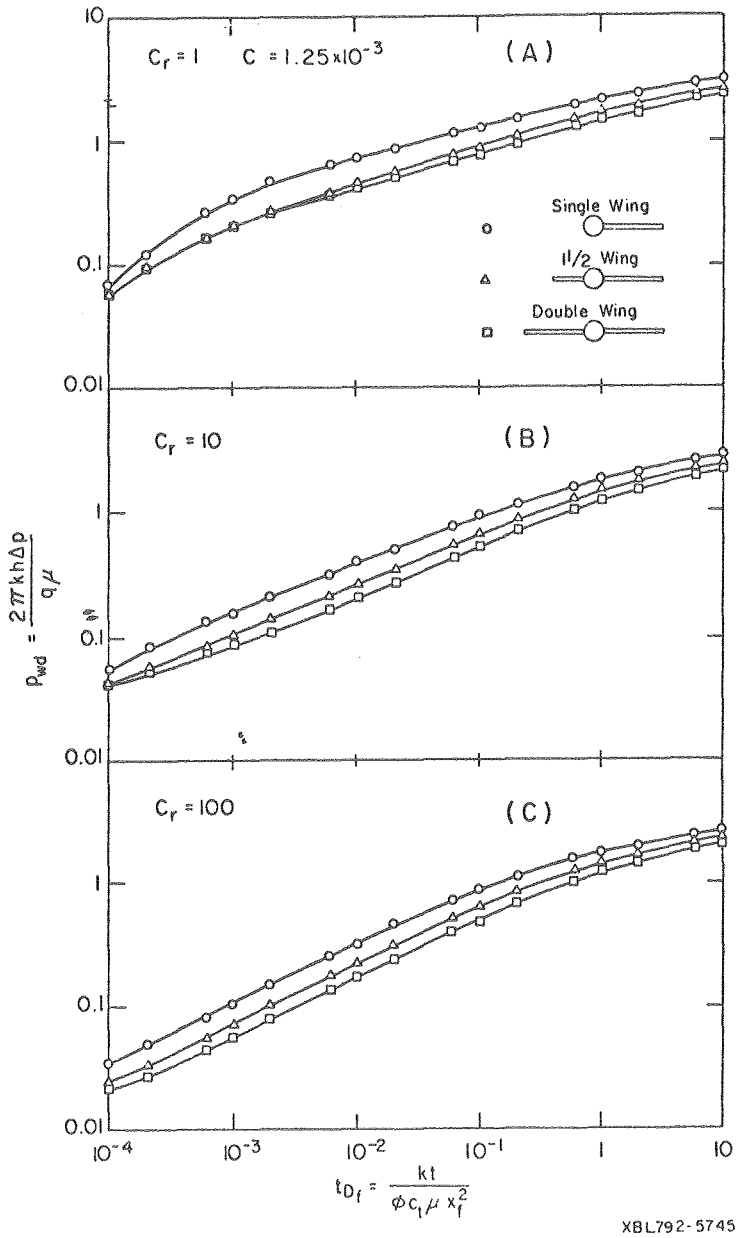

Fig. 8. Log-Log Plot of P_{wD} vs T_{Df} for Unequal Wing Length; for .005m Wellbore Radius and various Values of C_r.

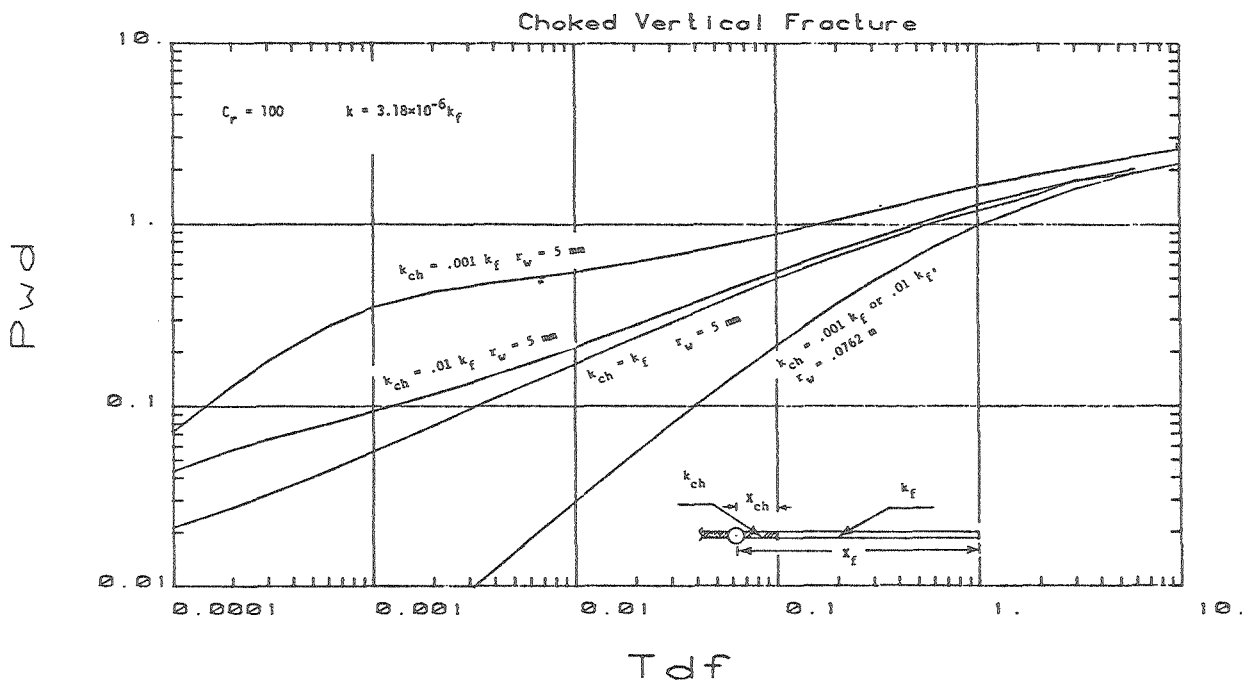

XBL 792-7377

Fig. 9. Log-Log Plot of P_{wD} vs T_{Df} for a Choked Vertical Fracture for Constant C_r, k, k_f, Wellbore Radii of .005 and .0762m.

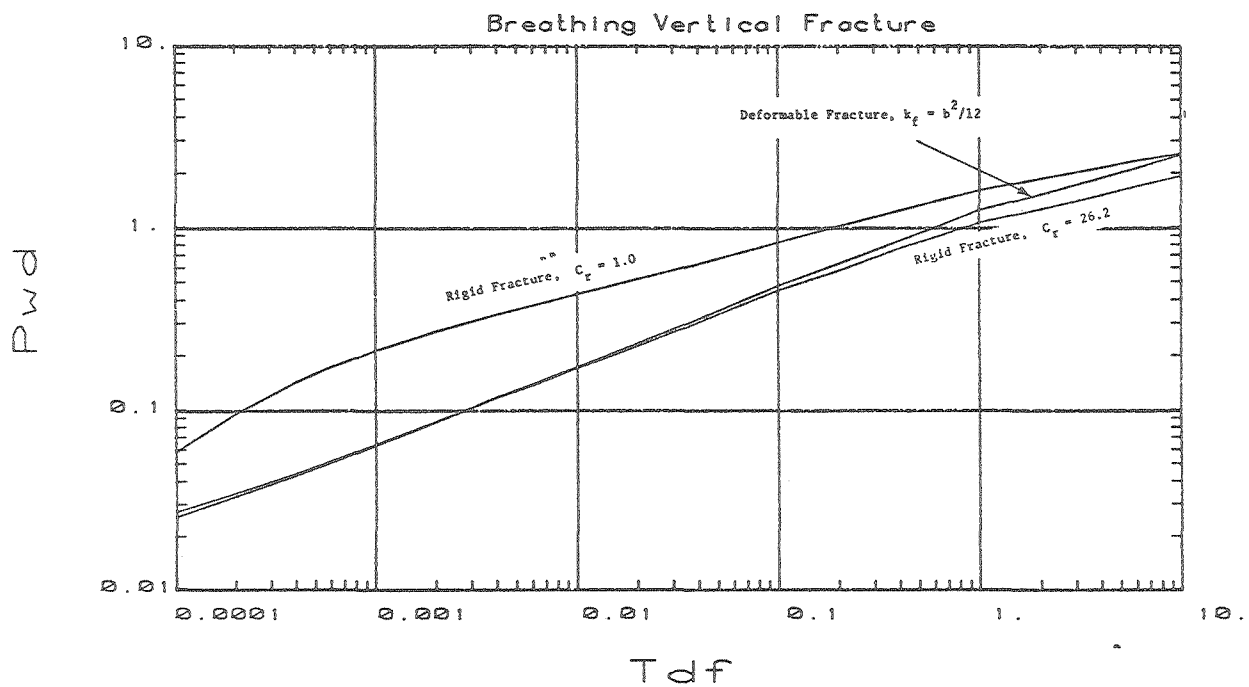

Fig. 10. Log-Log Plot of P_{wD} vs T_{Df} for a Breathing Vertical Fracture for r_w = .005m, W_o = .001m.

XBL 792-7378

This report was done with support from the Department of Energy. Any conclusions or opinions expressed in this report represent solely those of the author(s) and not necessarily those of The Regents of the University of California, the Lawrence Berkeley Laboratory or the Department of Energy.

TECHNICAL INFORMATION DEPARTMENT
LAWRENCE BERKELEY LABORATORY
UNIVERSITY OF CALIFORNIA
BERKELEY, CALIFORNIA 94720